J. Phys. Soc. Jpn.
Downloaded from journals.jps.jp by Shanxi University on 08/08/24

Journal of the Physical Society of Japan **93**, 094401 (2024)
https://doi.org/10.7566/JPSJ.93.094401

Quantum Correlations of Spin-wave-photon Pairs Produced from an Atomic Ensemble Coupled to a Ring Cavity

Haole Jiao[1,2], Minjie Wang[1,2], Jiajin Lu[1,2], Wenxin Fan[1,2], Zhifang Yang[1,2], Mengqi Xi[1,2], Shujing Li[1,2*], and Hai Wang[1,2]

[1]*The State Key Laboratory of Quantum Optics and Quantum Optics Devices, Institute of Opto-Electronics, Shanxi University, Taiyuan 030006, China*
[2]*Collaborative Innovation Center of Extreme Optics, Shanxi University, Taiyuan 030006, China*

(Received November 15, 2023; revised April 17, 2024; accepted July 8, 2024; published online August 8, 2024)

The quantum interface (QI) that generates non-classically-correlated pairs of spin-wave memories and photons is a building block (node) for DLCZ-like quantum repeater. The cross-correlation function, which characterizes quantum correlation of the pairs, and retrieval efficiency together with lifetime are important figures of merits of QIs. In this presented work, we generate highly retrievable spin-wave-photon pairs via cavity-enhanced DLCZ-like interaction between light and a cloud of cold atoms, where, the intrinsic retrieval efficiency reaches to ∼77.1% together with a memory lifetime of 0.65 ms. The cross-correlation functions of the pairs as a function of the storage time and excitation probability are measured, respectively. More important, we develop a theoretical model to describe the measured results in quantity. The theoretical model includes the cavity-enhanced noise coming from the imperfect readouts and is in agreement with the measured dependence of the cross-correlation function on the storage time and excitation probability.

1. Introduction

Quantum repeaters (QRs)[1)] hold promise for distributing entanglement over long distances (>1000 km) via optical fibers, thereby providing a feasible path to realize long-distance quantum communications[2,3)] and quantum networks.[4–7)] To realize a practical QR, Duan, Lukin, Cirac, and Zoller (DLCZ) proposed an attractive protocol,[1)] where, repeater nodes are formed by quantum interfaces (QIs) that generate non-classically-correlated pairs of spin-wave memories and Stokes photons via Spontaneous Raman Emissions (SREs) in atomic ensembles. For generating entanglement between two remote ensembles (nodes) belonging to a repeater link, the Stokes photons from the two ensembles are sent to the middle station between them. Conditioned on detection of a single photon after a beam splitter in the station, the two ensembles are entangled. After entanglement is generated over various links, the stored spin waves are mapped into photons for entanglement swapping. Along with the DLCZ scheme, many experiments have demonstrated the generation of the pair of correlated excitations via spontaneous Raman scattering (SRS).[8–22)] Also, the non-classically-correlated spin-wave-photon pairs[23–25)] can be achieved by using SPDC process together with "absorptive"[26)] quantum storages. In practical realization QRs, each node (quantum memory) is required to have highly retrieval efficiency, long storage time, multiplexed storage capacity and high quantum correlation characterized by cross-correlation function ($g^{(2)}$).[3,27)] In the past decade, the lifetime[12,13,15,16)] and retrieve efficiency[9,10,16,17)] of quantum memories have been significantly improved. For achieving long memory lifetime, two main decoherence processes which are caused by atomic motions[12,13)] and inhomogeneous broadening[11,13,14)] have been revealed. By suppressing the two decoherence processes, the storage times at $1/e$ retrieval efficiency for spin-wave QMs reach to ∼200 ms in optical-lattice atoms.[16)] The high-efficiency optical quantum memories have been achieved by using either high-optical-depth atomic ensembles[28–34)] or coupling moderate-optical-depth atoms with a low finesse optical cavity.[35–40)] Using the cavity-enhanced scheme, the achieved intrinsic retrieval efficiencies in DLCZ quantum memory are more than ∼76%.[16)]

For establishing entanglement in repeater links, atom-photon pairs are also required to have high quantum correlation ($g^{(2)}$), which enables one to achieve high-quality entanglement distribution between memories.[14)] In the past decade, the cross-correlation functions of the spin-wave-photon pairs as a function of the excitation probability or storage time have been experimentally demonstrated in atomic ensembles without cavity-enhanced retrieval.[10,20,41,42)] In Ref. 43 a simple theoretical model has been developed to describe the measured cross-correlation functions. For the spin-wave-photon QIs with a low-fineness optical cavity, the cross-correlation functions of the spin-wave-photon pairs as a function of excitation probability or storage time have been presented.[9,16)] However, in those works, no theoretical models have been developed to explain the measured results in quantity. The theoretical model that can quantitatively describe the dependence of the cross-correlation functions on the excitation probability and storage time are important for making the optimal entanglement distribution policies in QR.[43–45)] Yet, such a theoretical model is ambiguous. In the presented work, based on our highly retrievable spin-wave-photon pairs via cavity-enhanced DLCZ process in a cloud of cold atoms, we measure the cross-correlation function as a function of storage time and the excitation probability in experiment, respectively. We then propose a theoretical model that are in agreement with the experimental data.

2. Theoretical Model

When the atomic ensemble is placed in an optical cavity, the retrieval efficiency of the spin waves stored in the atomic ensemble can be improved. The cavity enhancement factor is expressed as

$$\mathcal{F} = \frac{(1-l)T}{\left[1-\sqrt{(1-l)R}\right]^2}. \tag{1}$$

where l is the intracavity loss and $R = 1 - T$ is the reflectivity of the output coupler (OC) of the cavity. The intrinsic

©2024 The Physical Society of Japan

J. Phys. Soc. Jpn.
Downloaded from journals.jps.jp by Shanxi University on 08/08/24

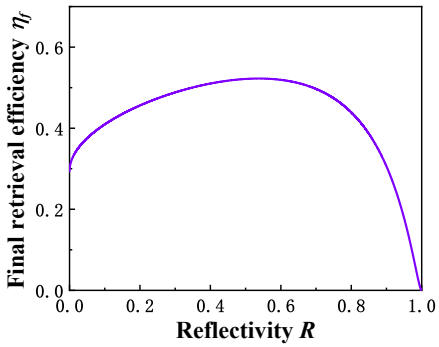

Fig. 1. (Color online) The final retrieval efficiency η_f as a function of the reflectivity R. The intracavity loss l is 15%, and the value of k is 0.6.

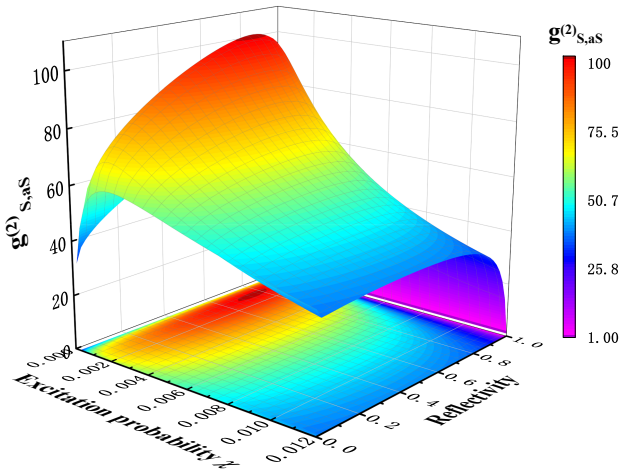

Fig. 2. (Color online) The cross-correlation $g^{(2)}_{S,aS}$ as a function of reflectivity R and excitation probability χ. The parameters are $l = 15\%$, $k = 0.6$, $\xi_{se} = 0.26$, $\eta_S = \eta_{aS} = 0.14$, $B = 0.0004$, and $C = 0.004$.

retrieval efficiency of atomic spins along the phase matching direction is written as

$$\gamma = \frac{k\mathcal{F}}{k\mathcal{F}+1} = \frac{k\dfrac{(1-l)T}{\left[1-\sqrt{(1-l)R}\right]^2}}{k\dfrac{(1-l)T}{\left[1-\sqrt{(1-l)R}\right]^2}+1}. \tag{2}$$

where k is a constant which related to optical depth and the atomic transition coefficients. Considering the escape efficiency of the cavity $\eta_o = \frac{T}{T+l}$, the final retrieval efficiency output from the cavity can be expressed as

$$\eta_f = \eta_o \gamma. \tag{3}$$

In our experiment, the intracavity loss $l = 15\%$ and the reflectivity of the OC $R = 80\%$, so the cavity enhancement factor is $\mathcal{F} = 5.5$. By substituting the measured values of retrieval efficiency $\gamma = 77\%$ into Eq. (2), the value of k can be inferred to be 0.6. To explore the relationship between the final retrieval efficiency η_f and the reflectivity R, we plot η_f as a function of R shown in Fig. 1. There is an optimal value of R to maximize the final retrieval efficiency η_f due to the existence of intracavity loss. With the increase of reflectivity, the intrinsic retrieval efficiency increases, but the escape efficiency decreases. The improvement of intrinsic retrieval efficiency is dominant in the case of small R, while the reduction of escape efficiency is dominant in the case of large R. Achieving the maximum final retrieval efficiency is a tradeoff between the intrinsic retrieval efficiency and the escape efficiency.

With cavity enhancement, the detection probability of Stokes photons P_S, the detection probability of anti-Stokes photons P_{aS}, and the probability of coincidence $P_{S,aS}$ between Stokes and anti-Stokes photons can be written as:

$$P_S = \chi\eta_S + B\eta_S, \tag{4}$$

$$P_{aS} = \chi\gamma(t)\eta_{aS} + N_{im} + C\eta_{aS}, \tag{5}$$

$$P_{S,aS} = \chi\gamma(t)\eta_{aS}\eta_S + P_S P_{aS}, \tag{6}$$

respectively, where χ is the excitation probability, η_S and η_{aS} are the total detection efficiencies for Stokes and anti-Stokes photons, respectively, $\gamma(t)$ is the intrinsic retrieval efficiency as a function of storage time, B (C) is the background noise in the detection channel for Stokes (anti-Stokes) photons, $N_{im} = \chi(1-\gamma(t))\xi_{se}A\eta_{aS}$ is the noise due to the imperfect retrieval efficiency, ξ_{se} is the branching ratio of the anti-Stokes photon atomic transition, $A = 2F/\pi$ represents the enhancement factor of the photon intensity output along the direction of the cavity mode caused by spontaneous emission, F is the fineness of the cavity. The intrinsic retrieval efficiency $\gamma(t)$ and the noise N_{im} are both increased by cavity, but the enhancement factors are different. The noise B (C) is mainly caused by the leakage of the write (read) light into the Stokes (anti-Stokes) detection channel. The write (read) light does not resonate with the cavity because has an angle with the Stokes (anti-Stokes) field. So, the values of B and C are not related with cavity parameters. The cross-correlation function between Stokes and anti-Stokes photons is

$$g^{(2)}_{S,aS} = \frac{P_{S,aS}}{P_S P_{aS}} \approx 1 + \frac{\gamma(t)}{(\chi+B)\gamma(t) + (\chi+B)(1-\gamma(t))\xi_{se}A + \dfrac{BC}{\chi} + C}. \tag{7}$$

According to the Eq. (7), we plot the cross-correlation function $g^{(2)}_{S,aS}$ as a function of the reflectivity of the OC R, shown in Fig. 2. For a fixed R, $g^{(2)}_{S,aS}$ achieves the maximum value $g^{(2)}_{\max,R}$ at $\chi \approx 0.0015$. $g^{(2)}_{\max,R}$ is 61.6 at $R = 0$, which corresponds to the case without cavity. $g^{(2)}_{\max,R}$ increase with the increase of R, and it reaches its peak of 103.4 at $R = 76.3\%$. It is obvious that the cavity has an enhancement effect for $g^{(2)}_{S,aS}$.

3. Experimental Setup

The experimental setup is shown in the schematic diagram Fig. 3(a). A cloud of cold atoms is placed in a ring cavity to be as memory medium. The cavity is formed by three high-reflective mirrors ($HR_{1,2,3}$) at 795 nm and an OC with reflectivity of 80%. The length and fineness of the cavity are $4.5m$ and 16, respectively. This locking beam comes from a semiconductor laser which also offers the state preparation light and is locked to the atomic transition $|5S_{1/2}, F = 2\rangle \rightarrow |5P_{1/2}, F = 2\rangle$. The locking beam is guided into the cavity by a beam splitter BS_3 with a reflectivity of 3%. Before injecting the cavity, the locking beam passes an acousto-optic modulator (AOM) and electro-optic modulator (EOM). By changing the modulation frequency of the AOM, the frequency of the locking beam is adjusted to resonate with

©2024 The Physical Society of Japan

J. Phys. Soc. Jpn.
Downloaded from journals.jps.jp by Shanxi University on 08/08/24

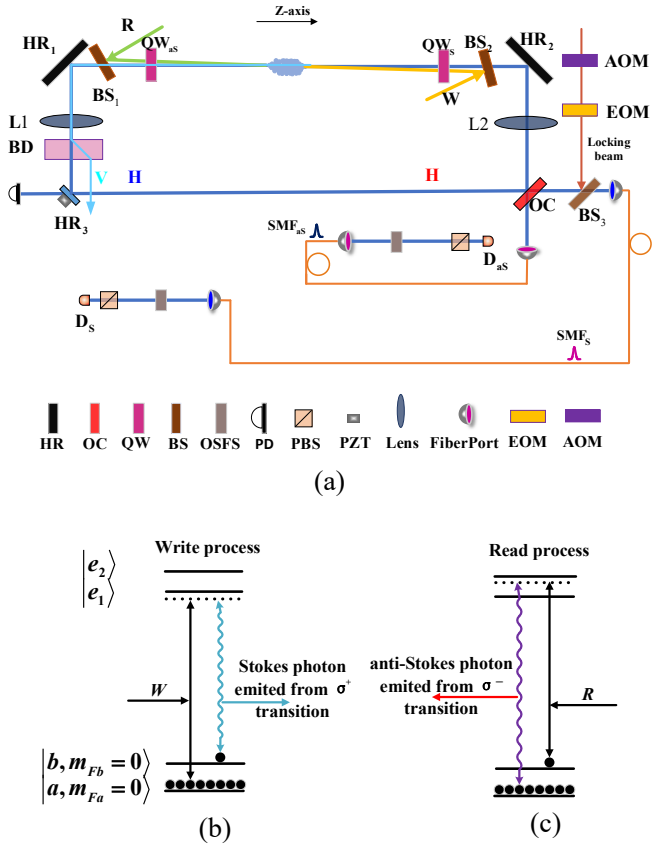

Fig. 3. (Color online) Schematic diagram for experimental setup. (a) shows the schematic diagram of our experimental setup, in which a cold ^{87}Rb atomic ensemble with an optical density of 16 is used as the memory medium. The ring cavity is formed by three high-reflection mirrors ($HR_{1,2,3}$) and an OC with reflectivity of 80%. To generate the pair of a Stokes photon and a spin wave, we apply a write pulse onto the atoms through the beam splitter BS_2. The spin wave is retrieved by applying a read beam which is directed to atoms through the beam splitter BS_1. A locking laser pulse is coupled to the V mode through a beam splitter (BS_3). The leakage of the cavity-locking pulse from HR_3 is detected by a fast photodiode (PD) to generate error signals. The error signal is amplified and used to drive a PZT to stabilize the cavity length. $OSFS$: optical-spectrum-filter set; BS_1 (BS_2): nonpolarizing beam splitter with a reflectivity of 3% (1%). AOM: acousto-optic modulator; EOM: electro-optic modulator.

the cavity. We use Pound–Drever–Hall (PDH) method to lock the cavity length. The locking beam passes the EOM for phase modulating to generate two sidebands. The light field transmitted from HR_3 is detected and converted to an electrical signal. The electrical signal is used to generate an error signal. To lock the cavity length, the error signal is feedbacked to the Piezoelectric transducer (PZT) mounted to HR_3 which changes the length of the PZT and the cavity length. We apply a bias magnetic field (4G) along z-direction to define quantum axis. Atomic levels related to the write (b) and read (c) processes in DLCZ scheme, respectively. The relevant atomic ground levels $|a\rangle = |5S_{1/2}, F = 1\rangle$ and $|b\rangle = |5S_{1/2}, F = 2\rangle$ together with the excited level $|e_1\rangle = |5P_{1/2}, F' = 1\rangle$ ($|e_2\rangle = |5P_{1/2}, F' = 2\rangle$) form a Λ-type system [Figs. 3(b) and 3(c)]. At first, the atoms are prepared in the Zeeman state $|a, m_{F_a} = 0\rangle$. Then, we start the generations of the spin-wave-photon pairs. Similar to that in our previous work,[37] we apply a right-circularly-polarized 795-nm write pulse with red-detuned by 110 MHz to the $|a, m_{Fa} = 0\rangle \rightarrow |e_1, m_{Fe_1} = 1\rangle$ transition to the atoms along z-axis through a beam splitter (BS_2) at the beginning of a trial. This write pulse induces Raman transition $|a, m_{Fa} = 0\rangle \rightarrow |b, m_{Fb} = 0\rangle$ via $|e_1, m_{Fe_1} = 1\rangle$ [Fig. 3(b)], which emits right-circularly-polarized (σ^+-polarized) Stokes photons and simultaneously creates SW excitations associated with the clock coherence $|m_a = 0\rangle \leftrightarrow |m_b = 0\rangle$. The write pulse also induces the Raman transition $|a, m_{Fa} = 0\rangle \rightarrow |b, m_{Fb} = 2\rangle$ via $|e_1, m_{Fe_1} = 1\rangle$, which emit left-circularly-polarized (σ^--polarized) Stokes photons into any of the cavity modes and simultaneously create magnetic-field-sensitive ($|m_{Fa} = 0\rangle \leftrightarrow |m_{Fb} = 2\rangle$) SWs. However, the σ^--polarized Stokes photon propagating along the counterclockwise direction will be transformed into an V (vertically) polarized photon by a $\lambda/4$-wave-plate QW_S and excluded from the cavity modes by BD, which removes the magnetic-field-sensitive SWs out our storage and promise the storage to have a longer lifetime. If the σ^+-polarized Stokes photon propagating along the counterclockwise direction is directed into the cavity mode, one collective excitation will be created in the cavity mode with wave-vector $k_M = k_w - k_S$, where k_w is the wave-vector of the write pulse and k_S that of the Stokes photon propagating in the cavity mode. For achieving a long-lived memory, we set the angle between the write and the Stokes fields to be small,[46] which is $\theta_R \approx 0.2^0$. In our presented experiment, the excitation probability $\chi \ll 1$ and the joint state of the spin-wave-photon pair is written:

$$|\psi\rangle = |0\rangle + \sqrt{\chi}|1\rangle_a|1\rangle_S + O(\chi), \tag{8}$$

where, $|1\rangle_S$ ($|1\rangle_a$) denotes a photon (a collective excitation) in Stokes (spin-wave) mode, $|0\rangle$ the vacuum state.

After a storage time t, we apply a read pulse that counter-propagates with the write beam. The read pulse is right-circularly polarized, which drives σ^--transition $|b, m_{Fb} = 0\rangle \rightarrow |e_2, m_{Fe_2} = -1\rangle$ and then converts the SW into an anti-Stokes photon with its wave vector determined by the phase-matched condition $k_{aS} = k_w - k_S + k_r \approx -k_S$, where, k_r and k_{aS} denote the wave vectors of the read laser pulse and anti-Stokes photon, respectively. The anti-Stokes photon is emitted on σ^--transition $|a, m_{Fa} = 0\rangle \rightarrow |e_2, m_{Fe_2} = -1\rangle$, which counter-propagates with the Stokes photon and is right-circularly-polarized. The right-circularly-polarized anti-Stokes photon is transformed into the V-polarized photon by a $\lambda/4$ plate named QW_{aS} (QW_S).

By precisely tuning the frequency detuning of the write and read laser beams, we make the Stokes and anti-Stokes fields simultaneously resonate with the ring cavity. Thus, atom-photon interaction is enhanced through the Purcell effect. As shown in Fig. 3(a), the escaping Stokes photon from the OC is coupled to a single-mode fiber SMF_S and then is directed to detector D_S. Before the detectors, we place optical-spectrum-filter sets to suppress noise from the write/read beams, and leakage from locking beam. The escaping anti-Stokes (retrieved) photon from the OC is coupled to a single-mode fiber SMF_{aS} and then is sent to single-photon detector D_{aS}.

4. Experimental Results

At first, we measure the retrieval efficiency of the spin-wave-photon pairs. The intrinsic retrieval efficiency is measured as $\gamma(t) = P_{S,aS}/(\eta_{aS}P_S)$, where, $P_{S,aS}$ denotes the probability of detecting a coincidence between the detectors

©2024 The Physical Society of Japan

J. Phys. Soc. Jpn.
Downloaded from journals.jps.jp by Shanxi University on 08/08/24

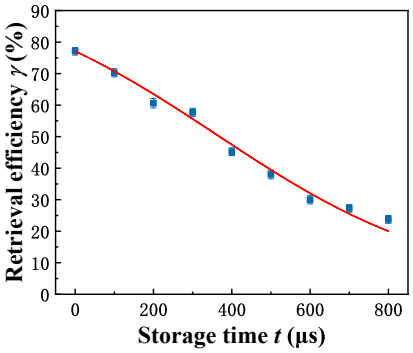

Fig. 4. (Color online) The measured retrieval efficiency (blue circles) as a function of storage time t. The solid red curve is the fitting to the retrieval efficiency according to $\gamma(t) = \gamma(0)(e^{-t/\tau} + e^{-t^2/\tau^2})/2$, yielding $\gamma(0) = 77\%$ and the lifetime $\tau \approx 654.7\,\mu s$, respectively.

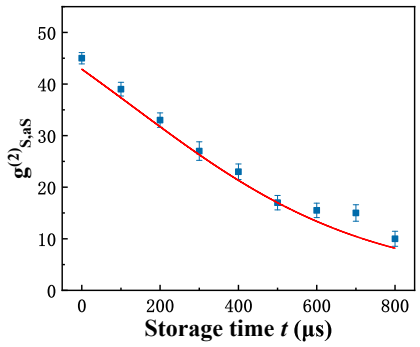

Fig. 5. (Color online) The measured $g^{(2)}_{S,aS}$ (blue squares) as a function of the storage time t. The solid red curve is the fitting to the $g^{(2)}_{S,aS}$ according to the Eqs. (7) and (9), where the fitting parameters are $\chi = 0.01$, $\gamma(0) = 77\%$, $A = 2 * F/\pi = 10$, $\xi_{se} = 0.26$, $B = 0.0004$, and $C = 0.004$.

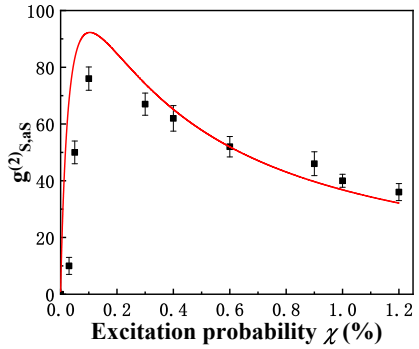

Fig. 6. (Color online) The measured $g^{(2)}_{S,aS}$ (black squares) as a function of the excitation probability χ. The solid red curve is the fitting to the $g^{(2)}_{S,aS}$ according to the Eq. (7), where the fitting parameters are $\gamma(0) = 70\%$, $A = 2 * F/\pi = 10$, $\xi_{se} = 0.26$, $B = 0.0004$, and $C = 0.004$.

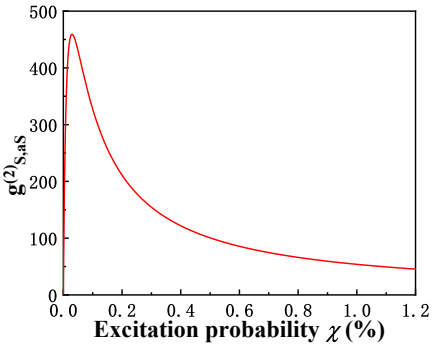

Fig. 7. (Color online) The theoretically calculated cross-correlation function as a function of the excitation probability for $\gamma(0) = 77\%$, $A = 2 * F/\pi = 10$, $\xi_{se} = 0.26$, $B = 0.0003$, and $C = 0.0004$.

D_S and D_{aS}, P_S donates the probability of detecting a photon at the detector D_S, $\eta_{aS} = \eta_{\rm cav}\eta_t\eta_D \approx 14\%$ is the total detection efficiency of read-out (anti-Stokes) channel, which includes the efficiency of light escaping from the ring cavity $\eta_{\rm cav} \approx 60\%$, the cavity-to-detector transmission efficiency $\eta_t \approx 34\%$, the efficiency of the single-photon detectors $\eta_D \approx 68\%$. Figure 4 plots the measured efficiency (blue circles) as a function of storage time t. The solid red curves are the fittings to the retrieval efficiency according to

$$\gamma(t) = \gamma(0)(e^{-t/\tau} + e^{-t^2/\tau^2})/2, \tag{9}$$

which yields zero-delay retrieval efficiency $\gamma(0) \approx 77.1\%$ and the lifetime $\tau \approx 654.7\,\mu s$, respectively.

Figure 5 plots the measured $g^{(2)}_{S,aS}$ (blue squares) as a function of the storage time t, showing that it decays with t. The reason for this is due to that the retrieval efficiencies decay with t. The red curve is the fitting to the data according to Eqs. (7) and (9), where, the values of the parameters $\chi = 0.01$, $A = 2 * F/\pi \approx 10$, $C = 0.004$, $B = 0.0004$ are taken from the measured data. The fitting parameter $\xi_{se} = 0.26$ is in agreement with that in previous work.[37)]

Figure 6 plots the measured $g^{(2)}_{S,aS}$ (blue squares) as a function of the excitation probability χ. The excitation probability is varied by changing the peak intensity of the write pulse. The measured results show that $g^{(2)}_{S,aS}$ decreases with the increase in χ when $\chi \geq 0.001$. However, when $\chi \leq 0.001$, $g^{(2)}_{S,aS}$ increases with the increase in χ, which has not been demonstrated in the previous results.[9)] We attributed this to the background noise in the anti-Stoke channel and imperfect retrieval.

To achieve spin-wave-photon pairs with a high cross-correlation function, we may further suppress the background noise B and C. Figure 7 plots the theoretically calculated $g^{(2)}_{S,aS}$ as a function of the excitation probability χ for the case that the values of B and C is very small, where the values of B and C are taken $B = 0.0003$, $C = 0.0004$. From Fig. 7 one can see that we a maximum $g^{(2)}_{S,aS} \approx 476$ will be obtained at $\chi = 0.0003$, which dependences on B and C.

5. Conclusion

In conclusion, we generate highly retrievable spin-wave-photon pairs via cavity-enhanced DLCZ-like interaction of light and a cloud of cold atoms. We obtain an intrinsic retrieval efficiency of ~77% and memory lifetime of 0.65 ms. We then measure the cross-correlation function as a function of the excitation probability. Our measured results show that the cross-correlation function reaches its maximum value at the special excitation probability, which has not been reported in previous works. By fitting the experimental data with a theoretical model, we explain our observed results well and find that the special excitation probability depends on background noise and imperfect retrieval.

©2024 The Physical Society of Japan

J. Phys. Soc. Jpn.
Downloaded from journals.jps.jp by Shanxi University on 08/08/24

Acknowledgment This work is supported by the National Natural Science Foundation of China (12174235), the Fund for Shanxi Key Subjects Construction (1331), and the Fundamental Research Program of Shanxi Province (202203021221011).

*lishujing@sxu.edu.cn

1) H. J. Briegel, W. Dur, J. I. Cirac, and P. Zoller, Phys. Rev. Lett. **81**, 5932 (1998).
2) L. M. Duan, M. D. Lukin, J. I. Cirac, and P. Zoller, Nature **414**, 413 (2001).
3) N. Sangouard, C. Simon, H. de Riedmatten, and N. Gisin, Rev. Mod. Phys. **83**, 33 (2011).
4) H. J. Kimble, Nature **453**, 1023 (2008).
5) C. Simon, Nat. Photonics **11**, 678 (2017).
6) S. Wehner, D. Elkouss, and R. Hanson, Science **362**, 303 (2018).
7) S. H. Wei, B. Jing, X. Y. Zhang, J. Y. Liao, C. Z. Yuan, B. Y. Fan, C. Lyu, D. L. Zhou, Y. Wang, G. W. Deng, H. Z. Song, D. Oblak, G. C. Guo, and Q. Zhou, Laser Photonics Rev. **16**, 2100219 (2022).
8) A. Kuzmich, W. P. Bowen, A. D. Boozer, A. Boca, C. W. Chou, L. M. Duan, and H. J. Kimble, Nature **423**, 731 (2003).
9) J. Simon, H. Tanji, J. K. Thompson, and V. Vuletic, Phys. Rev. Lett. **98**, 183601 (2007).
10) J. Laurat, H. de Riedmatten, D. Felinto, C. Chou, E. W. Schomburg, and H. J. Kimble, Opt. Express **14**, 6912 (2006).
11) D. Felinto, C. W. Chou, H. de Riedmatten, S. V. Polyakov, and H. J. Kimble, Phys. Rev. A **72**, 053809 (2005).
12) B. Zhao, Y.-A. Chen, X.-H. Bao, T. Strassel, C.-S. Chuu, X.-M. Jin, J. Schmiedmayer, Z.-S. Yuan, S. Chen, and J.-W. Pan, Nat. Phys. **5**, 95 (2009).
13) R. Zhao, Y. O. Dudin, S. D. Jenkins, C. J. Campbell, D. N. Matsukevich, T. A. B. Kennedy, and A. Kuzmich, Nat. Phys. **5**, 100 (2009).
14) J. Laurat, K. S. Choi, H. Deng, C. W. Chou, and H. J. Kimble, Phys. Rev. Lett. **99**, 180504 (2007).
15) A. G. Radnaev, Y. O. Dudin, R. Zhao, H. H. Jen, S. D. Jenkins, A. Kuzmich, and T. A. B. Kennedy, Nat. Phys. **6**, 894 (2010).
16) S.-J. Yang, X.-J. Wang, X.-H. Bao, and J.-W. Pan, Nat. Photonics **10**, 381 (2016).
17) E. Bimbard, R. Boddeda, N. Vitrant, A. Grankin, V. Parigi, J. Stanojevic, A. Ourjoumtsev, and P. Grangier, Phys. Rev. Lett. **112**, 033601 (2014).
18) M. Parniak, M. Dabrowski, M. Mazelanik, A. Leszczynski, M. Lipka, and W. Wasilewski, Nat. Commun. **8**, 2140 (2017).
19) H. Li, J.-P. Dou, X.-L. Pang, T.-H. Yang, C.-N. Zhang, Y. Chen, J.-M. Li, I. A. Walmsley, and X.-M. Jin, Optica **8**, 925 (2021).
20) K. B. Dideriksen, R. Schmieg, M. Zugenmaier, and E. S. Polzik, Nat. Commun. **12**, 3699 (2021).
21) C. Laplane, P. Jobez, J. Etesse, N. Gisin, and M. Afzelius, Phys. Rev. Lett. **118**, 210501 (2017).
22) K. Kutluer, M. Mazzera, and H. de Riedmatten, Phys. Rev. Lett. **118**, 210502 (2017).
23) D. Lago-Rivera, S. Grandi, J. V. Rakonjac, A. Seri, and H. de Riedmatten, Nature **594**, 37 (2021).
24) E. Saglamyurek, M. Grimau Puigibert, Q. Zhou, L. Giner, F. Marsili, V. B. Verma, S. Woo Nam, L. Oesterling, D. Nippa, D. Oblak, and W. Tittel, Nat. Commun. **7**, 11202 (2016).
25) K. T. Kaczmarek, P. M. Ledingham, B. Brecht, S. E. Thomas, G. S. Thekkadath, O. Lazo-Arjona, J. H. D. Munns, E. Poem, A. Feizpour, D. J. Saunders, J. Nunn, and I. A. Walmsley, Phys. Rev. A **97**, 042316 (2018).
26) K. Heshami, D. G. England, P. C. Humphreys, P. J. Bustard, V. M. Acosta, J. Nunn, and B. J. Sussman, J. Mod. Opt. **63**, 2005 (2016).
27) F. Bussières, N. Sangouard, M. Afzelius, H. de Riedmatten, C. Simon, and W. Tittel, J. Mod. Opt. **60**, 1519 (2013).
28) Y.-W. Cho, G. T. Campbell, J. L. Everett, J. Bernu, D. B. Higginbottom, M. T. Cao, J. Geng, N. P. Robins, P. K. Lam, and B. C. Buchler, Optica **3**, 100 (2016).
29) Y. F. Hsiao, P. J. Tsai, H. S. Chen, S. X. Lin, C. C. Hung, C. H. Lee, Y. H. Chen, Y. F. Chen, I. A. Yu, and Y. C. Chen, Phys. Rev. Lett. **120**, 183602 (2018).
30) P. Vernaz-Gris, K. Huang, M. Cao, A. S. Sheremet, and J. Laurat, Nat. Commun. **9**, 363 (2018).
31) Y. Wang, J. Li, S. Zhang, K. Su, Y. Zhou, K. Liao, S. Du, H. Yan, and S.-L. Zhu, Nat. Photonics **13**, 346 (2019).
32) J. Guo, X. Feng, P. Yang, Z. Yu, L. Q. Chen, C.-H. Yuan, and W. Zhang, Nat. Commun. **10**, 148 (2019).
33) O. Davidson, O. Yogev, E. Poem, and O. Firstenberg, Commun. Phys. **6**, 131 (2023).
34) M. Cao, F. Hoffet, S. Qiu, A. S. Sheremet, and J. Laurat, Optica **7**, 1440 (2020).
35) S. J. Yang, X. J. Wang, J. Li, J. Rui, X. H. Bao, and J. W. Pan, Phys. Rev. Lett. **114**, 210501 (2015).
36) X. J. Wang, S. J. Yang, P. F. Sun, B. Jing, J. Li, M. T. Zhou, X. H. Bao, and J. W. Pan, Phys. Rev. Lett. **126**, 090501 (2021).
37) M. Wang, S. Wang, T. Ma, Y. Li, Y. Xie, H. Jiao, H. Liu, S. Li, and H. Wang, Quantum **7**, 903 (2023).
38) L. Ma, X. Lei, J. Yan, R. Li, T. Chai, Z. Yan, X. Jia, C. Xie, and K. Peng, Nat. Commun. **13**, 2368 (2022).
39) M. Sabooni, Q. Li, S. Kroll, and L. Rippe, Phys. Rev. Lett. **110**, 133604 (2013).
40) P. Jobez, I. Usmani, N. Timoney, C. Laplane, N. Gisin, and M. Afzelius, New J. Phys. **16**, 083005 (2014).
41) J.-P. Dou, A.-L. Yang, M.-Y. Du, D. Lao, J. Gao, L.-F. Qiao, H. Li, X.-L. Pang, Z. Feng, H. Tang, and X.-M. Jin, Commun. Phys. **1**, 55 (2018).
42) S. Chen, Y. A. Chen, T. Strassel, Z. S. Yuan, B. Zhao, J. Schmiedmayer, and J. W. Pan, Phys. Rev. Lett. **97**, 173004 (2006).
43) B. Li, T. Coopmans, and D. Elkouss, IEEE Trans. Quantum Eng. **2**, 4103015 (2021).
44) Y. Wu, J. Liu, and C. Simon, Phys. Rev. A **101**, 042301 (2020).
45) Á. G. Iñesta, G. Vardoyan, L. Scavuzzo, and S. Wehner, npj Quantum Inf. **9**, 46 (2023).
46) S.-z. Wang, M.-j. Wang, Y.-f. Wen, Z.-x. Xu, T.-f. Ma, S.-j. Li, and H. Wang, Commun. Phys. **4**, 168 (2021).

©2024 The Physical Society of Japan